Molecular Cell, Volume *29*

Supplemental Data

Rad52 Promotes Postinvasion Steps of Meiotic Double-Strand-Break Repair

Jessica Lao, Steve Oh, Miki Shinohara, Akira Shinohara and Neil Hunter.

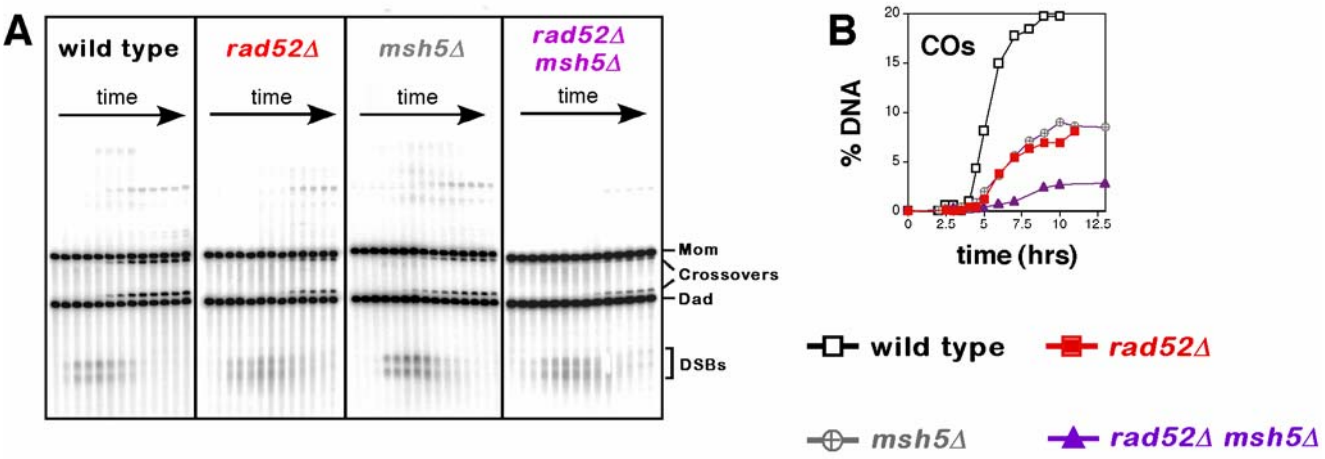

Figure S1. Crossovers in *rad52*Δ Mutants Are Promoted by the Pro-Crossover Factor, Msh5.

(A). Images of 1D gels from wild-type, *rad52*Δ*, msh5*Δ and *rad52*Δ *msh5*Δ time course experiments.

(B) Quantitation of crossovers (COs) in wild-type *rad52*Δ*, msh5*Δ and *rad52*Δ *msh5*Δ strains.

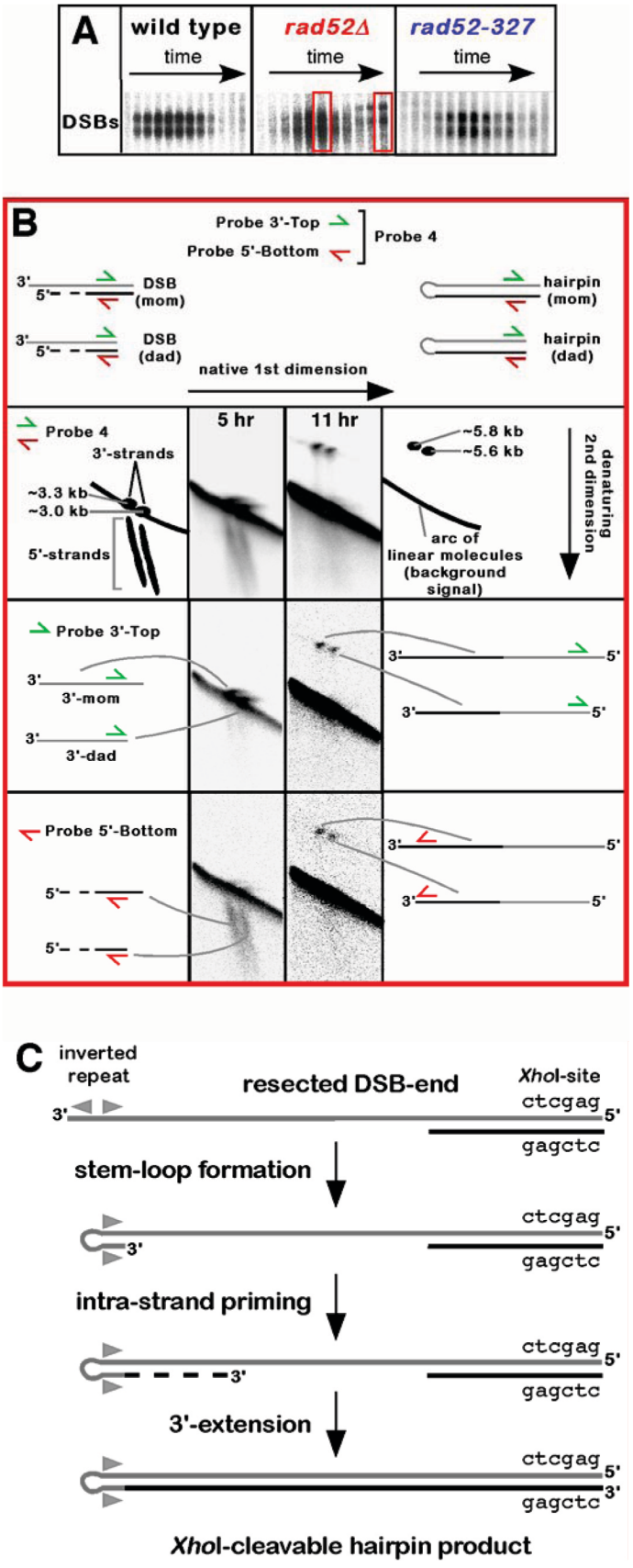
A
wild type
time
rad52Δ
time
rad52-327
time
DSBs
B
Probe 3'-Top
Probe 5'-Bottom
Probe 4
3'
5'
DSB
(mom)
DSB
(dad)
native 1st dimension
hairpin
(mom)
hairpin
(dad)
Probe 4
3'-strands
~3.3 kb
~3.0 kb
5'-strands
5 hr
11 hr
~5.8 kb
~5.6 kb
arc of
linear molecules
(background
signal)
denaturing
2nd dimension
Probe 3'-Top
3'-mom
3'-dad
Probe 5'-Bottom
C
inverted
repeat
resected DSB-end
XhoI-site
ctcgag
gagctc
stem-loop formation
intra-strand priming
3'-extension
XhoI-cleavable hairpin product

Figure S2. Strand Analysis of Late-Forming "DSB" Species in *rad52*Δ Cells.

(A) Dark exposures of the DSB regions from 1D gels (taken from Figure 2C). Red boxes highlight the 5 hr and 11 hr *rad52*Δ samples analyzed below in (B).

(B) Component strands of DSB signals from *rad52*Δ cells were examined using native/denaturing electrophoresis in which psoralen cross-links are removed prior to running a second dimension gel under denaturing conditions (Hunter and Kleckner, 2001).

First Row: Blots were successively hybridized with a probe that recognizes both strands of the DSB-ends (Probe 4 in Figure 1) and with strand-specific probes. Structures of normal DSB-ends and the proposed hairpin-ends under native conditions are shown.

Second Row: Analysis of DSBs from a 5 hr sample (when DSBs peak in *rad52*Δ cells) with Probe 4, reveals the expected composition of discrete signals that migrate on the arc of linear molecules, and smeared variable-length signals that migrate below the arc; these correspond, respectively, to the stable 3'-strands and variably resected 5'-strands of processed DSBs (Hunter and Kleckner, 2001). In contrast, the late-forming species, sampled at 11 hrs, produce only discrete hybridizing signals corresponding to single long strands of DNA. Under native conditions, however, these species are liberated by *Xho*I digestion, implying that double-stranded DNA is present at one or more *Xho*I recognition sites. In the second denaturing dimension, the two hybridizing species migrate above the arc of linears at positions corresponding to approximately 5.6 and 5.8 kb of single-stranded DNA. Sizes were estimated from three independent experiments by comparison to a ladder of known molecular weight markers using ImageQuant Version 5.0 software (Molecular Dynamics).

Third Row: Probe 3'-Top specifically hybridizes to the unresected 3'-strands of the DSBs in the 5 hr sample. This probe also recognizes the late-forming species in the 11 hr sample.

Fourth Row: Probe 5'-Bottom recognizes the variably resected 5'-strands of DSBs in the 5 hr sample and also hybridizes to the larger species from the 11 hr sample. The two strand-specific probes produce the same relative signal intensities for the late forming species indicating that these molecules contain equal numbers of 3'-5' and 5'-3' sequences.

C. Stem-loop model of hairpin formation at *HIS4LEU2* DSB-ends. The size and strand-composition of the late-forming species are consistent with a hairpin structure resulting from stem-loop formation and intramolecular priming within the 3'-strand of a DSB-end.

Sequence motifs with potential to form stem-loop structures in the 3'-strands of DSB-ends to the right of the *HIS4LEU2* DSB-site were identified using the stem-loop module of the GCG package (Accelrys, Software Inc.). The central *Bam*HI/*Ngo*MIV polymorphism, which marks the major DSB site (Figure 1), is at position 2958 (represented by a lower-case "t" in the sequences). All seven hairpin-loop motifs are within 0.5 kb of the DSB site. The first five motifs are within 34 bp of the DSB site.

Each motif is shown as its predicted stem-loop structure. Base-pairing within the stem is indicated by vertical lines. Loop bases are separated from the stem by a space. Numbers correspond to the length of the stem, the number of bases in the loop and an overall stability score for the stem-loop structure (the higher the number, the more stable the structure).

```
2955 GCCGGAtCCGGCTGCGC  TC    17 base stem, (stability score 36)
     |||||||||||| ||||
2992 TGGTCTAGGTCGTTGTG  CG    4 base loop


2931 CGTGGACGCGGCGG  CCATCGACT    14, (30)
     ||||| ||||||  |
2976 GCGCTCGCGTCGGC  CtAGGCCGG    18


2894 CACCGTGACCGCAG  AGGTTGAAGCT    14, (29)
     | ||||| |||| |
2943 GCGGCGCAGGTGCC  AACGGGTCGCG    22


2898 GTGACCGCAGAG  GTTGAAGCTGCGC    12, (24)
     ||| |||| | |              T
```

```
2948 TACCGGCGGCGC  AGGTGCCAACGGG    27


2676 GGTAGTGCCTT  GTGATCCG    11, (22)
     ||| ||||| |          G
2714 TCACCACGGCA  AGTTTAAT    17


2413 CGTTGACGTC  AGTGGAGGA    10, (21)
     ||||||| ||           C
2451 GTAACTGGAG  GCTAGACTA    19


2146 TTTGAACATC  CTCTTGTGCT    10, (21)
     |||||||| |
2185 AAACTTGTCG  CACTTCGAGT    20
```

Reference

Hunter, N., and Kleckner, N. (2001). The single-end invasion: an asymmetric intermediate at the double-strand break to double-holliday junction transition of meiotic recombination. Cell *106*, 59-70.

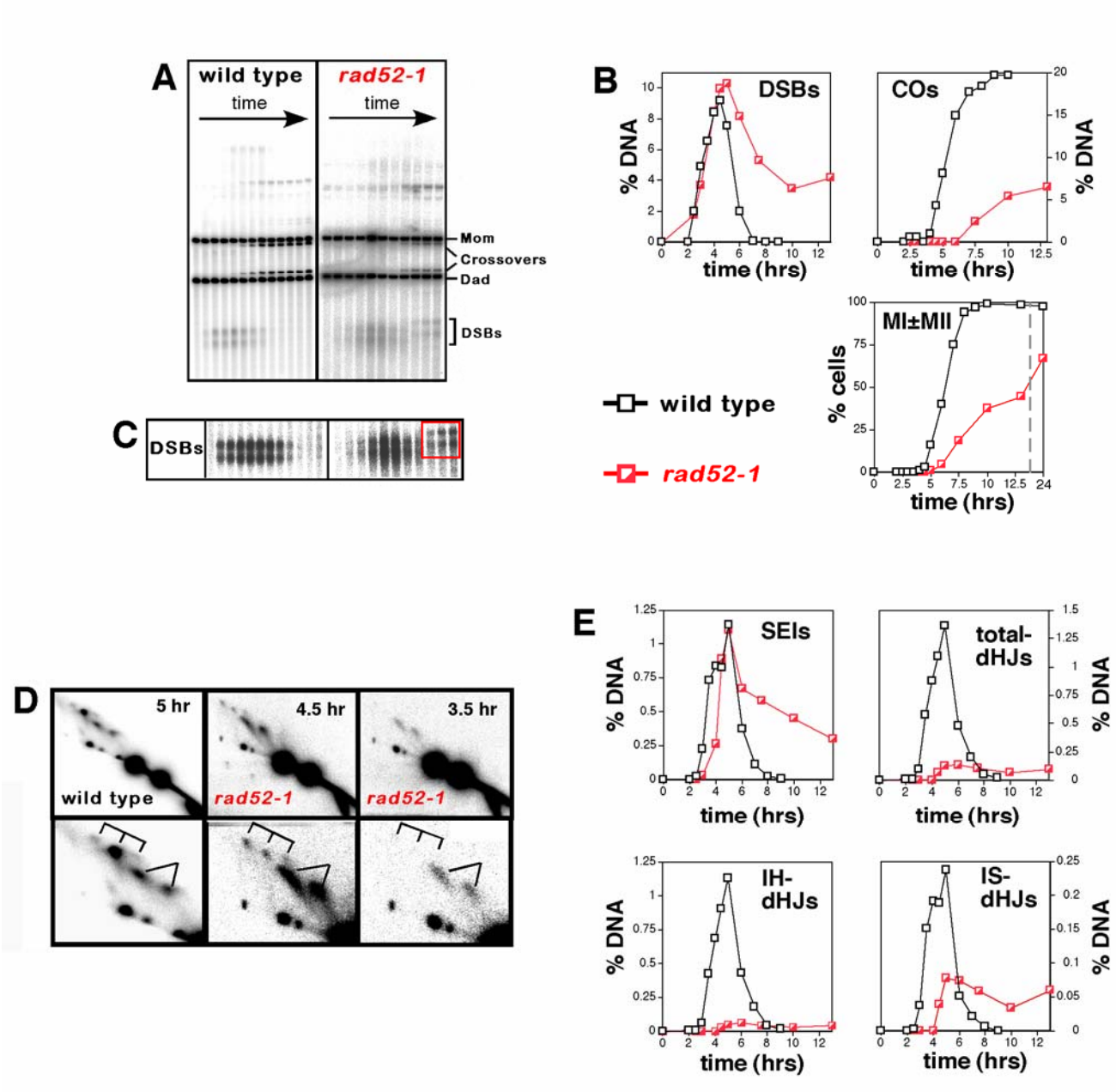

Figure S3. *rad52-1* mutants are defective for the SEI-to-dHJ transition.

(A) Images of 1D gels from wild-type and *rad52-1* time course experiments.

(B) Quantitation of DSBs and crossovers (COs), and analysis of meiotic divisions (MI±MII). The dashed grey line marks a break in the X-axis.

(C) Dark exposures of the DSB regions from 1D gels, highlighting the high molecular weight DSB species formed in *rad52-1* cells (see Figure S2).

(D) 2D analysis of JMs. In each case, a representative 2D panel is shown together with a blowup of the JM region. SEI and dHJ species are indicated by forked lines and tridents, respectively. The 3.5 hr time point from *rad52-1* shows SEI formation in the absence of detectable dHJs, a situation that is never observed in wild-type cells.

(E) Quantitation of JM formation.

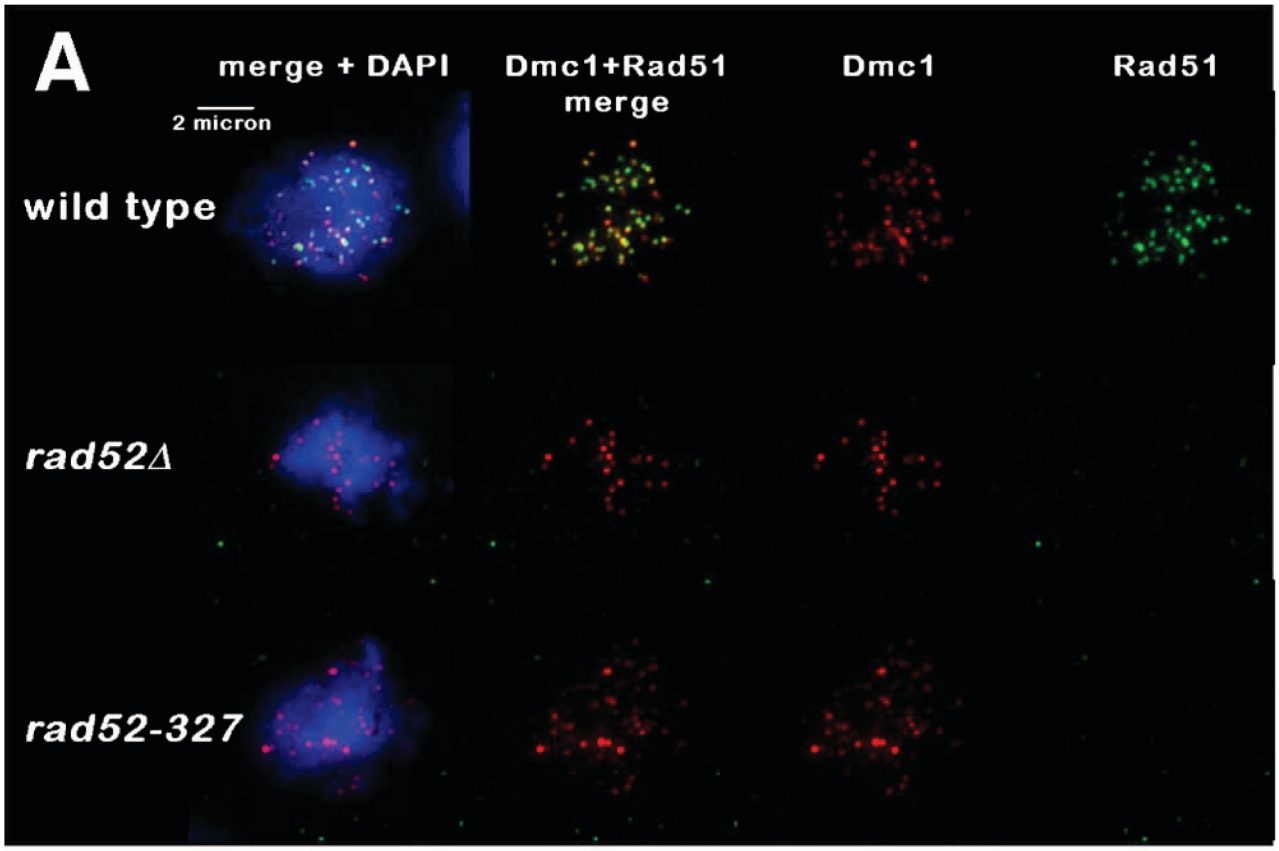
A
merge + DAPI
2 micron
Dmc1+Rad51 merge
Dmc1
Rad51
wild type
rad52Δ
rad52-327

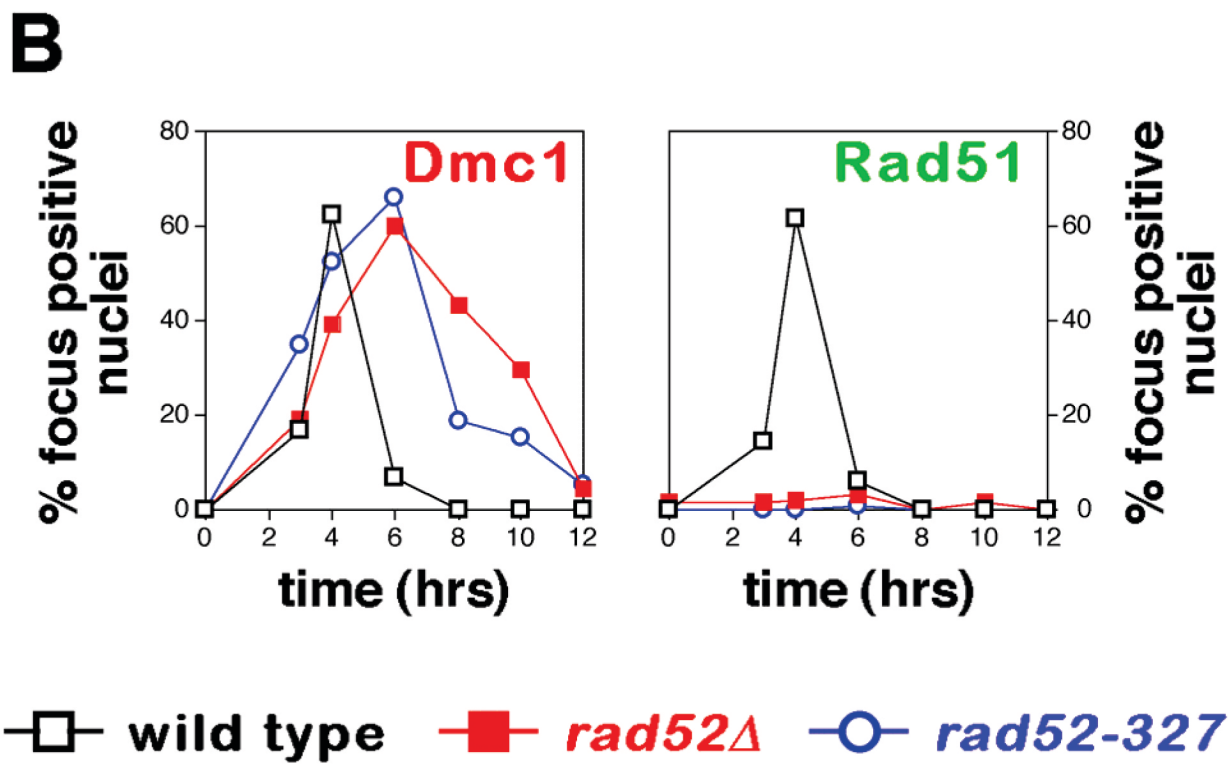
B
% focus positive nuclei
Dmc1
Rad51
time (hrs)
wild type
rad52Δ
rad52-327

Figure S4. Dmc1 Immunostaining Foci Assemble Along Meiotic Chromosomes Independently of Rad52 Mediator Function.

(A) Images of spread meiotic nuclei from wild-type, *rad52*Δ and *rad52-327* cells immunostained with antibodies against Dmc1 (red) and Rad51 (green).

(B) Quantitation of the percentage of focus-positive nuclei (containing greater than five foci) over time. ≥100 randomly selected nuclei were analyzed for each time point. The average numbers of Dmc1 foci per nucleus were 38 ± 10, 21 ± 7 and 15 ± 8 for wild type, *rad52*Δ and *rad52-327* strains, respectively. Reduced steady-state numbers of Dmc1 foci could reflect inefficient formation or asynchronous assembly of Dmc1 filaments in *rad52*Δ and *rad52-327* mutants.

Table S1. Strains used in this study.

Strain*	Genotype**
NHY452	*MAT**a**/MATa HIS4::LEU2-(Bam)/his4-X::LEU2-(Bam)–URA3 rad52-1/rad52-1*
NHY910	*MAT**a**/MATa HIS4::LEU2-(Bam)/his4-X::LEU2-(Bam)–URA3 rad52Δ::URA3/rad52Δ::URA3 dmc1Δ::kanMX4/dmc1Δ::kanMX4*
NHY1066	*MAT**a**/MATa HIS4::LEU2-(Bam)/his4-X::LEU2-(Bam)–URA3 rad51Δ::hisG/rad51Δ::hisG dmc1Δ::kanMX4/dmc1Δ::kanMX4*
NHY1226	*MAT**a**/MATa HIS4::LEU2-(BamHI)/his4-X::LEU2-(NgoMIV)–URA3 ndt80Δ::kanMX4/ndt80Δ::kanMX4*
NHY1296	*MAT**a**/MATa HIS4::LEU2-(BamHI)/his4-X::LEU2-(NgoMIV)–URA3*
NHY1698	*MAT**a**/MATa HIS4::LEU2-(BamHI)/his4-X::LEU2-(NgoMIV)–URA3 rad52-327/rad52-327 dmc1Δ::kanMX4/dmc1Δ::kanMX4*
NHY1711	*MAT**a**/MATa HIS4::LEU2-(BamHI)/his4-X::LEU2-(NgoMIV)–URA3 rad52-327/rad52-327*
NHY1721	*MAT**a**/MATa HIS4::LEU2-(BamHI)/his4-X::LEU2-(NgoMIV)–URA3 rad52Δ::URA3/rad52Δ::URA3*
NHY1831	*MAT**a**/MATa HIS4::LEU2-(BamHI)/his4-X::LEU2-(NgoMIV)–URA3 msh5Δ::kanMX4/msh5Δ::kanMX4*
NHY1950	*MAT**a**/MATa HIS4::LEU2-(BamHI)/his4-X::LEU2-(NgoMIV)–URA3 rad52Δ::hphMX4/rad52Δ::hphMX4 msh5Δ::kanMX4/msh5Δ::kanMX4*
NHY2556	*MAT**a**/MATa HIS4::LEU2-(BamHI)/his4-X::LEU2-(NgoMIV)–URA3 ndt80Δ::kanMX4/ndt80Δ::kanMX4 rad52Δ::hphMX4/rad52Δ::hphMX4*
NHY2567	*MAT**a**/MATa HIS4::LEU2-(BamHI)/his4-X::LEU2-(NgoMIV)–URA3 ndt80Δ::kanMX4/ndt80Δ::kanMX4 rad52-327/rad52-327*

*All strains are isogenic derivatives of SK1.

**All strains are also homozygous for the mutations *ura3Δ(sma-pst)* and *leu2::hisG.*